Uniaxial stress study of the 1026-meV center in Si:Pt

J. P. Leitão* and M. C. Carmo
Department of Physics, University of Aveiro, 3810-193 Aveiro, Portugal

M. O. Henry and E. McGlynn
School of Physical Sciences, National Centre for Plasma Science and Technology, Dublin City University, Collins Avenue, Dublin 9, Ireland

(Received 19 January 2001; published 31 May 2001)

The luminescence of the 1026-meV optical center, observed in silicon doped with platinum by implantation, was studied under uniaxial stress. The splitting patterns show a complex behavior, especially for the main directions ⟨100⟩ and ⟨110⟩. In the ⟨100⟩ direction, nonlinear shifts in energy are seen for some components in addition to changes in the intensities. At liquid-helium temperatures, increasing the stress permits the observation of higher-energy transitions. For this center, a model with trigonal symmetry is proposed in which the system has four excited states, three doubly degenerate and one nondegenerate. The three zero phonon lines of the center correspond to transitions of the type $A \leftrightarrow E$ and are polarized in the plane XY of the center. The transition involving the nondegenerate excited state is forbidden by the selection rules. The application of uniaxial stress causes interaction between the excited states.

DOI: 10.1103/PhysRevB.63.235208 PACS number(s): 71.70.Fk, 78.55.Ap, 71.55.Cn

I. INTRODUCTION

Platinum as an impurity in silicon is widely studied due to its applications in the electronic industry in the lifetime control of minority carriers in silicon devices.[1] This impurity introduces several levels in the forbidden band gap both of *n*- and *p*-type material (Refs. 1–3 and the references therein). Some of these levels act as traps for the carriers.

Several studies show a large number of defects involving one or more platinum atoms[4–9] and, in some cases, other impurities.[10–14] The usual way of doping the material is by diffusion at high temperatures. This method has the disadvantage of poor control of the level of the impurity introduced into the lattice and favors the formation of aggregates over simpler defects. The implantation of impurity ions offers a much better control of the concentrations in the material. However, above a certain dose, the implantation process leads to amorphization of the lattice and so care must be taken not to go beyond this level. The observed defects were studied mostly by electron paramagnetic resonance (EPR).[7,8,10–12,15] Nevertheless, other experimental techniques have been used, namely photoluminescence[5,6,16] and optical absorption.[9,14,17]

In this work, we doped the silicon material by ion implantation with a dose near but below the amorphization level. The luminescence of the 1026-meV optical center was studied under variable temperatures and application of uniaxial stress. A model that describes the splitting patterns under this external field is discussed.

II. EXPERIMENTAL DETAILS

In this work, we used samples grown by the Czochralski method and of both *p* and *n* type. The dimensions were approximately $2\times4\times12$ mm, with the longest edge along the main directions ⟨100⟩, ⟨110⟩, and ⟨111⟩. All the samples were etched ($HF:H_2NO_3$ in the ratio 1:10) after a mechanical polishing. The ion implantation was done at room temperature with Pt^+ ions of energy 170 keV with a dose in the range $(1-8.9)\times10^{13}$ cm^{-2}. The values for the maximum concentration of the impurity, calculated with the PROFILE CODE program,[18] were between 3.1×10^{18} and 2.8×10^{19} cm^{-3}, and the depth of this maximum was 625 Å. After the implantation, the samples were annealed at high temperatures to activate the luminescence. After each anneal, the samples were rapidly quenched to room temperature.

The emission from the samples was acquired in two types of spectrometer. The first one was a Spex 1000M dispersive monochromator and the second one a Brucker 66v spectrometer. Both spectrometers were equipped with a Ge diode detector cooled to liquid nitrogen temperature. Photoluminescence was excited with the 488-nm line from an argon laser.

The stress measurements were made in the Fourier spectrometer equipped with a stress cell inside an Oxford CF1204 cryostat.

III. RESULTS AND DISCUSSION

A. Optimization of the luminescence

It was shown previously[16] that the doping of silicon with platinum by ion implantation with additional annealing results in the formation of three optical centers designated by the energy of the zero phonon lines in each center: 777, 884, and 1026 meV. The 1026-meV center was observed in *p*-type material and the best conditions for its production were established as an annealing for 4 min at 900°C.

B. Description of the center

The 1026-meV optical center shows at low temperature (4.2 K) two ZPL at 1024.1 and 1026.9 meV. For $T>10$ K, another ZPL is observed at 1030.9 meV. At lower energies, transitions involving a phonon of 10.3 meV are observed. This low energy for this local mode suggests the participa-

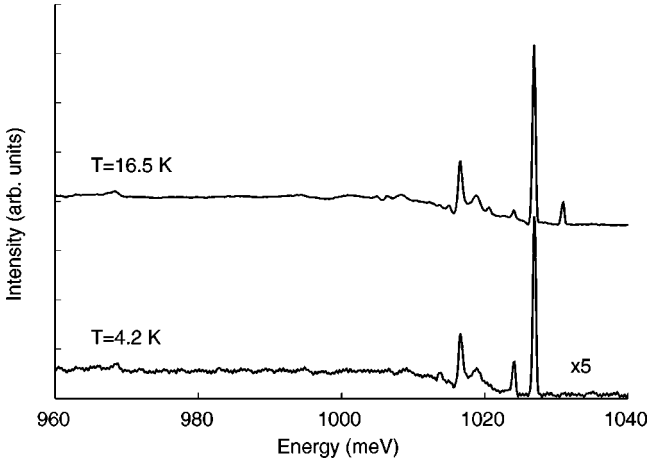

FIG. 1. Photoluminescence of the 1026-meV optical center at 4.2 and 16.5 K. The sample is *p*-type and was implanted with Pt^+ ions of energy 170 keV with a dose of 10^{13} cm^{-2}.

tion in the defect of impurities with mass higher than that of the silicon atoms. Also at lower energy, a vibronic band is seen with a small intensity and maximum at ~35 meV from the ZPL, which shows some similarity with the continuum spectrum of the lattice. A phonon replica involving the TO lattice mode is also observed. No phonon replicas are observed in the anti-Stokes region. In Fig. 1, we show the photoluminescence at 4.2 and 16.5 K.

The emission spectrum can be calculated with linear coupling electron-phonon theory.[19] Coupling to the local mode of 10.3 meV and to the lattice modes with the Huang-Rhys factors of 0.5 and 2.6, respectively, was considered. The agreement with the experimental spectrum is quite good, as shown in Fig. 2. The calculated relaxation energy of the lattice is $E_R = 91$ meV.

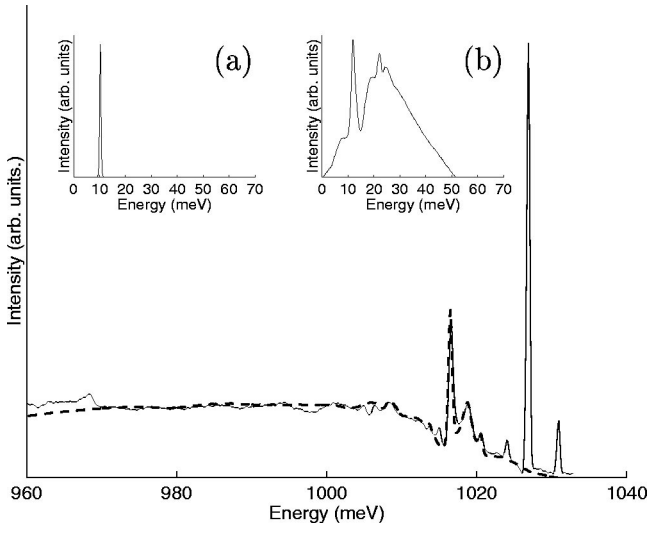

FIG. 2. Comparison of experimental (full line) and theoretical (broken line) emission of the 1026-meV optical center at 16.5 K. The insets (a) and (b) show, respectively, the local mode of 10.3 meV and the continuum spectrum of lattice modes considered in the reconstruction of the emission spectrum.

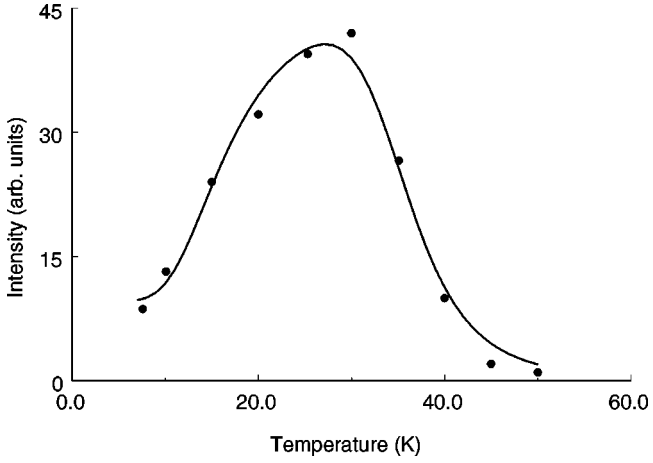

FIG. 3. Dependence on the temperature of the integrated intensity of the ZPL in the center 1026 meV. The line represents the fit of Eq. (1) to the experimental points ($E = 34.6$ meV, $C = 70\,000$, $E_{nr} = 5.8$ meV, $g = 4.2$, and $b = 241$).

C. Temperature dependence

The increase of the sample temperature causes an increase of the integrated intensity in the ZPL (Fig. 3). A maximum is reached at ~30 K and a subsequent reduction is observed for higher temperatures with complete extinction at ~50 K. The initial increase is attributed to the competition for the capture of free excitons between the luminescent defects and nonradiative shallow defects.[20] The increase of the temperature promotes the release of excitons bound to the nonradiative defects, making them available for the capture by the other defects, including the luminescent ones. The experimental behavior can be described by the following equation:[20]

$$\frac{I(T)}{I(0)} = \left\{ \left[1 + C \exp\left(-\frac{E}{kT} \right) \right] (1+f) \right\}^{-1},$$

$$f = \frac{g}{1 + b \exp\left(-\frac{E_{nr}}{kT} \right)}, \tag{1}$$

where f represents the fraction of the nonradiative centers that have not bound an exciton and can hence compete with the luminescent centers for the capture of the free excitons. This term includes the temperature-independent ratio of the capture cross sections for excitons at the luminescent centers and the competing defects. E represents the thermal ionization energy of the luminescent center and E_{nr} the thermal ionization energy of the nonradiative defects.

The fit to the experimental points is shown in Fig. 3, where $E = 34.6$ meV and $E_{nr} = 5.8$ meV. The thermal ionization energy is considerably higher than the usual values obtained for isoelectronic defects (~15 meV). However, this behavior is not unique. For example, the ''*ABC*'' center related to aluminum[21] shows a value of ~44 meV.

Taking the free-exciton energy of 1155.7 meV, we obtain a spectroscopic localization energy of $1155.7 - 1026.9 = 128.8$ meV for the center. Considering the thermal ioniza-

tion energy of 34.6 meV, we have a residual localization energy of 94.2 meV. This value is very near the relaxation energy of the lattice (91 meV) calculated above. The proximity of the two values indicates that the first particle is bound with a consequent relaxation of the lattice and the second particle is bound in the resulting field.

The temperature dependence of the relative intensities of the ZPL could be fitted by an Arrhenius relation. The fit to the experimental measurements resulted in infinite temperature ratios of $I_1:I_2:I_3=1:83:86$. So, the transition probabilities from the two higher levels are approximately two orders of magnitude higher than from the lower excited level. The energy separations calculated from the fit, 7.0 and 2.8 meV, respectively, are near the experimental values.

This electronic level structure suggests an excitonic nature for the center. However, the high value obtained for the thermal ionization energy (34.6 meV) is unusual for centers of this kind.

D. Uniaxial stress measurements

The application of uniaxial stress (P) was done at low temperature ($\sim$4.2 K) for $P\|[001]$ and for $P\|[111]$, and at a higher temperature (15-20 K) for $P\|[110]$. Due to the higher temperature in the last direction, the ZPL at 1030.9 meV was observed in the absence of the external perturbation. The obtained splitting patterns are shown in Fig. 4, and, with the exception of $P\|[111]$, they are quite complex.

For $P\|[001]$, each ZPL splits into two components. In the range of low stress, the slopes are linear and approximately symmetric. For $P>30$ MPa, two new components (''*e*'' and ''*f*'') appear at higher energy. The components ''*d*'' and ''*e*'' interact and, as a consequence, repel each other around 40 MPa. In the range $80-100$ MPa, the ''*b*'' component interacts with the next higher component. The above interactions provoke changes in the intensity of the components and cause the slopes to be nonlinear.

The extrapolation to zero stress of the components ''*e*'' and ''*f*'' indicates that their origin is at 1029.5 and 1030.9 meV. This relates the component ''*f*'' with the higher-energy excited state. For the component ''*e*,'' no state was observed near 1029.5 meV when the temperature was raised. So the transition involving this state must be forbidden.

At low temperatures, the ZPL at 1026.9 meV has approximately five times the intensity of the ZPL at 1024.1 meV. This fact puts more uncertainty in the measurement of the intensity of the components resulting from the ZPL with lower energy. At a stress value of 11.8 MPa, the relative intensities are $I_a:I_b=4:2$ and $I_c:I_d=3:2$.

The application of uniaxial stress along [111] results in the splitting of the two lower-energy ZPL into three components each. In the range of stress values studied, no components were observed for the higher-energy states. The observed slopes are linear, which suggests the absence of interactions between the excited states. The measurement of the relative intensities of each component for a stress value of 92.4 MPa resulted in the values $I_h:I_\alpha:I_i=17:6:22$ and $I_j:I_\beta:I_k=11:6:18$.

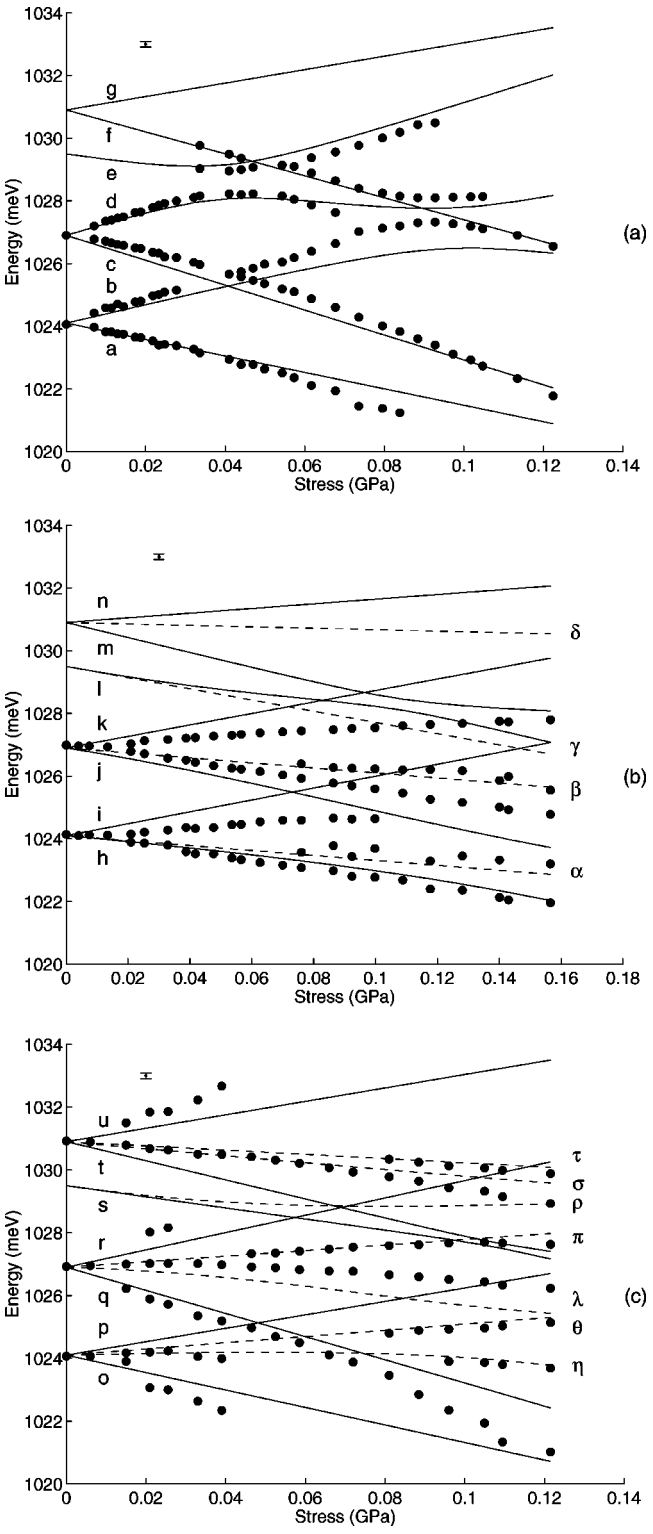

FIG. 4. Fan diagrams for the 1026-meV under uniaxial stress. (a) $P\|[001]$. The lines represent the fit of the proposed model for all defect orientations. (b) $P\|[111]$. The broken lines represent the fit for the orientation 1 and the full lines represent the fit for the orientations 2, 3, and 4. (c) $P\|[110]$. The full lines represent the fit for the orientations 1 and 2 and the broken lines represent the fit for the orientations 3 and 4. Each component is labeled by a letter: roman for the full lines and greek for the broken lines.

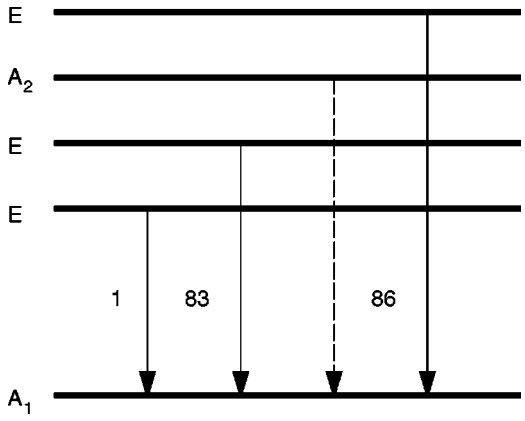

FIG. 5. Proposed model for the 1026-meV center. The symmetry of the center is trigonal (C_{3v}) and it has four excited states. Three of them are doubly degenerate transforming as E states and the other one is a nondegenerate state transforming as an A_2 state. The ground state transforms as an A_1 state. The full lines represent transitions that are allowed and the broken line a forbidden one. Near each allowed transition is the relative transition probability.

For $P\|[110]$, the sample temperature was higher than for the other two directions, which allowed the observation of the higher-energy state at 1030.9 meV at zero stress. The observed splitting patterns are quite complex, as shown in Fig. 4. At this temperature, the spectrum is dominated by the ZPL at 1026.9 meV, the other two ZPL having much less intensity. The line at 1026.9 meV splits in four components, whereas for the other two states fewer components are observed due to the reduced intensity. However, the observed shift rates are very similar for the three states.

The energy and intensity of some of the components are difficult to measure experimentally due to the strong overlap resulting in line broadening even for small values of stress. For a stress value of 72.0 MPa, the relative intensities of the three components were $I_\pi : I_\lambda : I_q = 1.3:2.7:1.3$.

E. Theoretical model

To explain the observed splitting patterns, we propose for this center a model in trigonal symmetry (C_{3v}) where the ground state is an A_1 state and there are four excited states, three E states, and one A_2 state. Experimentally it is not possible to distinguish the previous model from another one where the ground state and the nondegenerate excited state transforms as A_2 and A_1, respectively. Because from the point of view of the uniaxial stress experiments the two models are equivalent, we will consider the first one (Fig. 5). The transition from the A_2 state to the A_1 ground state is forbidden by the selection rules. However, the application of uniaxial stress promotes mixing between the different excited states, and for $P\|[001]$ the transition originating at 1029.5 meV becomes observed for stress values higher than ~ 30 MPa.

The uniaxial stress perturbation is described in local coordinates by

$$V = C_{A_1}(S_{XX}+S_{YY}+S_{ZZ}) + \tfrac{1}{2}C'_{A_1}(2S_{ZZ}-S_{XX}-S_{YY}) + C_{E_\theta}(S_{YY}-S_{XX}) + 2C_{E_\varepsilon}S_{XY} + 2C'_{E_\theta}S_{XZ} + 2C'_{E_\varepsilon}S_{YZ}, \tag{2}$$

where $S_{ij} = P\, n_i\, n_j$ are the stress tensor components, P being the applied stress and n_i the cosine of the angle between the direction of application of the stress and the local axis i, and $C_{A_1} \cdots C'_{E_\varepsilon}$ are electronic operators with transformation properties given by the labels. The secular matrix is given by

$$|V_{ij} - E\,\delta_{ij}| = 0, \tag{3}$$

where $V_{ij} = \langle \phi_i | V | \phi_j \rangle$ is the matrix element of the Hamiltonian [Eq. (2)] calculated between the states $|\phi_j\rangle$ and $|\phi_i\rangle$. The calculation of their eigenvalues and eigenstates is done in the set of four excited states. The basis functions are the eigenfunctions of each state: $|E^1_\theta\rangle$, $|E^1_\epsilon\rangle$, $|E^2_\theta\rangle$, $|E^2_\epsilon\rangle$, $|A_2\rangle$, $|E^3_\theta\rangle$, and $|E^3_\epsilon\rangle$. The secular matrix takes the form given in Table I.

In a lattice of T_d symmetry, a trigonal center has four possible nonequivalent orientations (Table II). For $P\|[001]$, all the orientations of the center are equivalent, but for $P\|[111]$ and $P\|[110]$ the solutions of the secular matrix (Table I) depend on the orientation of the center considered. In the first case ($P\|[111]$), the degeneracy is not lifted for the first orientation, whereas for the other orientations the

TABLE I. Secular matrix for the model of the uniaxial stress perturbation considering the model of Fig. 5. The parameters are given by the following expressions, where the label i characterizes the particular E state in each matrix element: $c^i_1 = a^i_1(S_{XX}+S_{YY}+S_{ZZ}) + \frac{1}{2}a^i_2(2S_{ZZ}-S_{XX}-S_{YY})$; $c^i_2 = a^i_3(S_{YY}-S_{XX}) + 2a^i_4 S_{XZ}$; $c^i_3 = -2a^i_3 S_{XY} - 2a^i_4 S_{YZ}$; $\alpha^i = -2d^i S_{XY} - 2f^i S_{YZ}$; $\beta^i = d^i(S_{YY}-S_{XX}) + 2f^i S_{XZ}$; $w = g(S_{XX}+S_{YY}+S_{ZZ}) + \frac{1}{2}h(2S_{ZZ}-S_{XX}-S_{YY})$.

	$\|E^1_\theta\rangle$	$\|E^1_\epsilon\rangle$	$\|E^2_\theta\rangle$	$\|E^2_\epsilon\rangle$	$\|A_2\rangle$	$\|E^3_\theta\rangle$	$\|E^3_\epsilon\rangle$
$\|E^1_\theta\rangle$	$E_1+c^1_1+c^1_2$	c^1_3	0	0	α^1	0	0
$\|E^1_\epsilon\rangle$	c^1_3	$E_1+c^1_1-c^1_2$	0	0	β^1	0	0
$\|E^2_\theta\rangle$	0	0	$E_2+c^2_1+c^2_2$	c^2_3	α^2	0	0
$\|E^2_\epsilon\rangle$	0	0	c^2_3	$E_2+c^2_1-c^2_2$	β^2	0	0
$\|A_2\rangle$	α^1	β^1	α^2	β^2	E_3+w	α^3	β^3
$\|E^3_\theta\rangle$	0	0	0	0	α^3	$E_4+c^3_1+c^3_2$	c^3_3
$\|E^3_\epsilon\rangle$	0	0	0	0	β^3	c^3_3	$E_4+c^3_1-c^3_2$

TABLE II. Orientations for a trigonal center in a lattice of T_d symmetry.

Orientation	X	Y	Z
1	$[11\bar{2}]$	$[\bar{1}10]$	$[111]$
2	$[\bar{1}\bar{1}2]$	$[1\bar{1}0]$	$[\bar{1}\bar{1}1]$
3	$[1\bar{1}2]$	$[\bar{1}\bar{1}0]$	$[1\bar{1}\bar{1}]$
4	$[\bar{1}12]$	$[110]$	$[\bar{1}\bar{1}\bar{1}]$

solutions of the secular matrix are equal. For $P\|[110]$, we obtain a solution for the first two orientations different from the solution for the last two orientations.

The best fit to the experimental points is characterized by the set of parameters in Table III and given by the lines in Fig. 4.

From Fig. 4, we see that the splitting patterns are quite well described by the proposed model. For $P\|[001]$, the nonlinear slopes of the components ''*b*'' and ''*d*'' as well as those of the components that appear for high energy are described. In the case of $P\|[111]$, the fit is poor for the two components with higher slope. For $P\|[110]$, in spite of the high number of components, the fit is globally acceptable. The fit is poorer for the components ''*o*,'' ''*r*,'' and ''*u*'' that experimentally have a low intensity.

The proposed model for the center considers the interaction between the four excited states. For each particular stress value, the eigenstates are linear combinations of the basis functions. The intensity of each component depends on each linear combination. However, when the stress value is low enough, the intensities must be near the ones predicted in the absence of any interaction between the excited states. For $P\|[001]$, the theoretical relative intensities of the two components are 3.3:2. The experimental values are closer to the above intensities for the ZPL at 1026.9 meV than for the ZPL at 1024.1 meV. The low intensity for the latter ZPL does not allow a proper comparison with the theoretical intensities.

For $P\|[111]$, the theoretical relative intensities for three components are given by 9:6:17. The experimental values for the intensities of the two ZPL are near these values, again being less accurate for the line at 1024.1 meV.

For $P\|[110]$, the direction of the detection of the emission light was $[\bar{1}10]$. Considering the electric dipole with equal intensity along the local X and Y axes, the relative intensities of the four components, ordered by descending slope, should be $2:\frac{4}{3}:2:0$. Experimentally, the intensity of the component with higher slope in the splittings of the ZPL at 1026.9 meV is very small. On the other hand, the component with lower slope was clearly visible. This could be caused by a slight misalignment of the sample geometry with respect to the optical axis of the system.

With increasing stress, the intensities of the components are well described by the model, in particular the changes in intensity of some components for $P\|[001]$. The contribution of the $|A_2\rangle$ basis function to the component ''*d*'' increases and this component becomes progressively forbidden until it disappears at ~ 70 MPa. For higher stress values, the fitted ''*b*'' and ''*d*'' components repel each other as observed experimentally for the ''*b*'' component and the component

TABLE III. Parameters that characterize the best fit to the experimental splitting patterns.

$E_1 = 1024.1$ meV	$a_1^1 = 1.7$ meV GPa^{-1}
$E_2 = 1026.9$ meV	$a_2^1 = -9.6$ meV GPa^{-1}
$E_3 = 1029.5$ meV	$a_3^1 = 3.4$ meV GPa^{-1}
$E_4 = 1030.9$ meV	$a_4^1 = 27.2$ meV GPa^{-1}
$a_1^2 = -1.1$ meV GPa^{-1}	$a_1^3 = -6.8$ meV GPa^{-1}
$a_2^2 = -6.9$ meV GPa^{-1}	$a_2^3 = 4.5$ meV GPa^{-1}
$a_3^2 = 6.5$ meV GPa^{-1}	$a_3^3 = 2.3$ meV GPa^{-1}
$a_4^2 = 36.4$ meV GPa^{-1}	$a_4^3 = 28.3$ meV GPa^{-1}
$d^1 = 10.3$ meV GPa^{-1}	$d^2 = 15.1$ meV GPa^{-1}
$f^1 = 4.2\times10^{-2}$ meV GPa^{-1}	$f^2 = 2.7$ meV GPa^{-1}
$d^3 = 2.0$ meV GPa^{-1}	$g = -17.9$ meV GPa^{-1}
$f^3 = -1.2\times10^{-2}$ meV GPa^{-1}	$h = 1.4\times10^{-2}$ meV GPa^{-1}

TABLE IV. Eigenstates for the ''*b*,'' ''*d*,'' and ''*e*'' components for $P\|[001]$. The more significant contributions for each component are indicated in percentages.

Stress (MPa)	$\|E_\epsilon^1\rangle$	$\|E_\epsilon^2\rangle$	$\|A_2\rangle$
	''*b*'' component		
67.7	94.9	0.3	4.8
79.5	88.0	0.9	11.2
88.4	77.7	1.7	20.6
97.3	62.4	3.1	34.5
101.7	54.0	3.9	42.1
113.5	34.8	5.5	59.7
122.4	25.3	6.1	68.6
	''*d*'' component		
7.0	0	99.8	0
27.7	0	91.9	8.0
33.6	0.1	83.2	16.7
44.0	0.5	58.3	41.2
49.9	1.0	44.8	54.2
57.3	2.1	32.7	65.2
67.7	4.8	22.9	72.3
92.8	29.0	11.8	59.2
104.7	51.1	8.0	40.9
	''*e*'' component		
7.0	0	0.2	99.8
27.7	0.2	8.1	91.7
33.6	0.3	16.8	82.9
44.0	0.4	41.7	57.9
49.9	0.4	55.2	44.4
57.3	0.4	67.2	32.4
67.7	0.4	76.8	22.8
92.8	0.4	85.8	13.8
104.7	0.4	87.6	12.0

with lower slope from the ZPL at 1030.9 meV. Table IV shows the eigenstates associated with the ''*b*,'' ''*d*,'' and ''*e*'' components for some stress values as given by the model. In each splitting, the eigenstate of the component with lower slope is always given by just one basis function: ''*a*'' component – $|E_\theta^1\rangle$; ''*c*'' component – $|E_\theta^2\rangle$; ''*f*'' component – $|E_\theta^3\rangle$.

For the other two directions of uniaxial stress, $P\|[111]$ and $P\|[110]$, the role of the A_2 state is not so important, due to the weaker interactions between the four excited states. In the case of $P\|[111]$ and for the first orientation of the center, the model gives three states doubly degenerate (''α,'' ''β,'' and ''δ'' components) and one state nondegenerate (''γ'' component). This eigenstate shows no mixture of the E states with the A_2 state. The remaining components are due to the other possible orientations for the center. The ''*i*,'' ''*k*,'' and ''*n*'' components are always given by the $|E_\theta^1\rangle$, $|E_\theta^2\rangle$, and $|E_\theta^3\rangle$ basis functions, respectively. For the other components, the increase of the stress causes a progressive interaction between them, but for the range of stress values studied, this interaction is small. The only exception is the range 100 -120 MPa, where the ''*l*'' and ''*m*'' components interact somewhat. So, the lack of observation of transitions involving the two higher excited states is explained by the model.

In the splitting pattern for $P\|[110]$, it is only possible to analyze the ZPL at 1026.9 meV due to the low intensities of the other two ZPL. Let us consider the first two orientations of the center. The ''*p*,'' ''*r*,'' and ''*n*'' components are given by the $|E_\theta^1\rangle$, $|E_\theta^2\rangle$, and $|E_\theta^3\rangle$ basis functions, respectively. The other four components have a low interaction with the exception of the ''*s*'' and ''*t*'' components in the range $90-130$ MPa. However, in spite of the latter interaction, the ''*s*'' component, initially forbidden, never receives a sufficient contribution to become observable. Considering the last two orientations for the center, the ''*o*,'' ''π,'' and ''τ'' components are given by the $|E_\theta^1\rangle$, $|E_\theta^2\rangle$, and $|E_\theta^3\rangle$ basis functions, respectively. The ''σ'' component is essentially given by the $|E_\epsilon^3\rangle$ basis function. The other three components show, with the increase of the applied stress, a progressive mixture of the $|E_\epsilon^1\rangle$, $|E_\epsilon^2\rangle$, and $|A_2\rangle$ basis functions. However, the ''ρ'' component still remains essentially forbidden and the other two components essentially allowed.

Other optical centers related to transition-metal impurities show a trigonal symmetry.[22–25] To make possible a comparison between the different sets of parameters in each center, all these sets of parameters must be written in the same type of coordinates. In crystalline coordinates, the perturbation is written in terms of four parameters: A_1, A_2, B, and C.[26] Transforming our set of parameters to the crystalline coordinates results in $A_1=2$, $A_2=-5$, $B=14$, and $C=19$ meV GPa^{-1}. The A_1 and A_2 values are near the ones obtained for the 735- (Si:Au+Fe), 1014- (Si:Cu), and 838-meV (pair Cr-B) centers. The magnitude of B is also near the values obtained for these centers. For $P\|\langle 111\rangle$, the splittings and the shift rates of the observed components make the 1026-meV center very similar to other centers of excitonic nature, such as the ''*ABC*'' center related to aluminum.[22]

Overall, the removal of the electronic degeneracy for $P\|\langle 111\rangle$, the near equivalence of the thermal ionization energies, the electronic level structure, and relative transition probabilities suggest a great similarity between the 1026-meV and the ''*ABC*'' centers.

IV. CONCLUSIONS

The 1026-meV center was studied by photoluminescence under uniaxial stress. The results showed evidence for the existence of four excited states. The observed zero phonon transitions occur from doubly degenerate excited states to the ground state. The fourth state is a nondegenerate one and the transition to the ground state is forbidden by the selection rules. The symmetry of the center is trigonal, the observed ZPL's corresponding to A↔E transitions. The lower excited state has a relative transition probability approximately two orders of magnitude lower than the relative transition probabilities for the other degenerate excited states.

*Electronic address: quim@fis.ua.pt

[1] K.P. Lisiak and A.G. Milnes, J. Appl. Phys. **46**, 5229 (1975).
[2] A.A. Gill, N. Baber, and M.Z. Iqbal, J. Appl. Phys. **67**, 1130 (1990).
[3] H. Zimmermann and H. Ryssel, Appl. Phys. Lett. **58**, 499 (1991).
[4] H.H. Woodbury and G.W. Ludwig, Phys. Rev. **126**, 466 (1962).
[5] G. Armelles, J. Barrau, M. Brousseau, and J.P. Noguier, Phys. Rev. B **33**, 1243 (1986).
[6] G. Armelles, J. Barrau, V. Thomas, and M. Brousseau, J. Phys. C **19**, 2593 (1986).
[7] F.G. Anderson, R.F. Milligan, and G.D. Watkins, Phys. Rev. B **45**, 3279 (1992).
[8] U. Juda and M. Höhne, Solid State Phenom. **47-48**, 293 (1996).
[9] M. Kleverman, J. Olajos, and P. Tidlund, Phys. Rev. B **56**, 1376 (1997).
[10] M. Höhne, U. Juda, Yu.V. Martynov, T. Gregorkiewicz, C.A.J. Ammerlaan, and L.S. Vlasenko, Phys. Rev. B **49**, 13 423 (1994).
[11] M. Höhne and U. Juda, Mater. Sci. Technol. **11**, 680 (1995).
[12] O. Scheerer, M. Höhne, U. Juda, and H. Riemann, J. Appl. Phys. **82**, 3456 (1997).
[13] J.-U. Sachse, J. Weber, and E.Ö. Sveinbjörnsson, Phys. Rev. B **60**, 1474 (1999).
[14] M. Kleverman, X. Zhang, and J. Olajos, Physica B **273-274**, 449 (1999).
[15] P. Alteheld, S. Greulich-Weber, J.-M. Spaeth, H. Weihrich, H. Overhof, and M. Höhne, Phys. Rev. B **52**, 4998 (1995).
[16] E. Alves, J. Bollmann, M. Deicher, M.C. Carmo, M.O. Henry, M.H.A. Knopf, J.P. Leitão, R. Magerle, and C.J. McDonagh, Mater. Sci. Forum **258-263**, 473 (1997).
[17] G. Davies, E.C. Lightowlers, P. Izard, and M. Brousseau, Mater. Sci. Eng., B **4**, 173 (1989).
[18] PROFILE CODE, Implant Sciences Corporation, Wakefield, MA, 1997.
[19] D.B. Fitchen, in *Physics of Color Centers*, edited by W.B. Fowler (Academic, New York, 1968), Chap. 5.
[20] G. Davies, Phys. Rep. **176**, 83 (1989).

[21] J. Weber, W. Schmid, and R. Sauer, Phys. Rev. B **21**, 2401 (1980).
[22] G. Davies, J. Phys. C **17**, 6331 (1984).
[23] R. Sauer and J. Weber, Physica B & C **116B**, 195 (1983).
[24] H. Conzelmann, Appl. Phys. A: Solids Surf. **42**, 1 (1987).
[25] M. C. Carmo (private communication).
[26] A.E. Hughes and W.A. Runciman, Proc. Phys. Soc. London **90**, 827 (1967).